AGU ADVANCING EARTH AND SPACE SCIENCE

Earth's Future

RESEARCH ARTICLE
10.1029/2022EF002670

Compound Post-Fire Flood Hazards Considering Infrastructure Sedimentation

Ariane Jong-Levinger[1], Tirtha Banerjee[1], Douglas Houston[2], and Brett F. Sanders[1,2]

[1]Department of Civil and Environmental Engineering, University of California, Irvine, CA, USA, [2]Department of Urban Planning and Public Policy, University of California, Irvine, CA, USA

Key Points:

- Post-fire flooding represents a compound hazard based on interdependence between fire, runoff, and infrastructure sedimentation
- A new modeling framework is formulated and applied to simulate compound post-fire flood hazards using stochastic inputs
- Compound post-fire flood hazards can be up to an order of magnitude greater than flood hazards in the absence of fire

Supporting Information:

Supporting Information may be found in the online version of this article.

Correspondence to:

A. Jong-Levinger,
arianej@uci.edu

Citation:

Jong-Levinger, A., Banerjee, T., Houston, D., & Sanders, B. F. (2022). Compound post-fire flood hazards considering infrastructure sedimentation. *Earth's Future*, *10*, e2022EF002670. https://doi.org/10.1029/2022EF002670

Received 28 JAN 2022
Accepted 12 JUL 2022

Abstract Flood and debris hazards are heightened following wildfires, but are challenging to quantify due to interdependence between fire frequency and severity, runoff and sediment fluxes during storms, and sedimentation that reduces infrastructure capacity. Herein we present a stochastic simulation framework to estimate compound flood and debris hazards from sequences of wildfires and rainstorms and the accumulation of sediment within flood infrastructure. Application of the framework to a hypothetical watershed representative of southern California shows that the present-day compound hazard may be up to 6 times greater than the marginal hazard posed by peak flows in the absence of wildfire, and that future compound hazards could be up to 11 times greater than the marginal hazard based on future increases in wildfire frequency. Numerous sensitivities are investigated, including infrastructure design and maintenance, which are shown to be crucial for moderating future increases in post-fire flood hazards.

Plain Language Summary More frequent and intense wildfires lead to increased risks of flooding and debris hazards following rainstorms. However, existing models for estimating hazards to communities do not account for the filling of protective flood infrastructure with sediment, which reduces capacity. We present an original model for estimating post-fire flood and debris hazards that captures the interconnected influences of wildfire, rainstorms, and reduced infrastructure capacity from sedimentation. The modeling approach can simulate present and future hazards to aid both short-term and long-term risk management efforts. Simulations show that present-day hazards are up to six times greater based on the interaction of processes compared to flood hazards in the absence of fires. Based on future increases in wildfire frequency, future flood hazards could be up to 11 times greater. Simulations also show that hazards can be reduced with more intensive cleaning and maintenance.

1. Introduction

Mediterranean and semi-arid regions with mountainous topography are exposed to post-fire flood hazards that are extremely dangerous (Jennings & Brooks, 1982; National Research Council, 1996). Herein we use "flood hazards" to refer to mixtures of water, sediment, rock, and other debris which are sometimes described as "debris hazards" or "flood and debris hazards." High-velocity flows with sediment, debris, and uncertain flow paths can cause devastating losses of life and property, such as the Montecito, CA debris event in 2018 which took 23 lives and damaged over 400 homes (Kean et al., 2019), and the 1976 flood in La Paz, Mexico where a sediment-laden flood carved a new flow path through the city center and killed thousands (Sanders & Grant, 2020). Runoff and erosion on burnt terrain have been observed to be 1–4 orders of magnitude greater than that on unburnt terrain in the European Mediterranean and more than 100 times greater on large-plot to hillslope scales in the southwestern United States (Shakesby, 2011; Williams et al., 2014). These hydrogeomorphic changes result from the removal of vegetation cover by wildfire, which exposes soil to erosion via raindrop impact, and, in some cases, from the creation of a hydrophobic layer caused by heat-induced soil water repellency and/or the clogging of soil pores with ash (Hyde et al., 2017; Moody et al., 2013). Three major trends point to increasing post-fire flood risks in the southwestern United States: first, wildfires are becoming more frequent and more severe (Dennison et al., 2014; Li & Banerjee, 2021; Westerling et al., 2006); second, precipitation extremes are intensifying (Gershunov et al., 2019; Swain et al., 2018), and even relatively minor storms can trigger debris flows shortly after burn events (Kean & Staley, 2021; Staley et al., 2013); and third, development is expanding below and into mountain wildlands where post-fire flood hazards are concentrated (Cannon & DeGraff, 2009; Radeloff et al., 2018).

Considerable research has focused on predictive models of post-fire peak flows and sediment yields to improve the understanding of risks and to design infrastructure to mitigate hazards. Post-fire sediment yield has largely been estimated using empirical relationships (Gartner et al., 2014; Kampf et al., 2016; Kean & Staley, 2021; Pelletier & Orem, 2014; Wagenbrenner & Robichaud, 2014), while a smaller number of process-based models exist (Goodrich et al., 2012; Robichaud et al., 2007). Studies comparing empirical and process-based models have not yielded clear evidence for a single approach that consistently performs well (Chen et al., 2013; Kinoshita et al., 2014). In the United States, the post-fire flood hazard models most widely used operationally are those developed by the United States Geological Survey to predict debris flow probability and volume (Cannon et al., 2010; Gartner et al., 2014; Kean & Staley, 2021; Staley et al., 2016, 2017). These empirical models were trained and tested using observations from over 300 debris flow events that occurred in several states in the western United States, the majority of them in southern California. Southern California is especially vulnerable to debris flow hazards based on combinations of steep topography, frequent wildfires, expansive urban development, and intense precipitation (Kean & Staley, 2021).

Urban areas at risk of exposure to post-fire flood and debris hazards have been estimated in a number of ways for emergency preparedness measures such as risk communication to exposed populations, the placement of protective walls and barriers, and evacuation plans. Two-dimensional (2D) models for mud and debris flow hazards emerged in the 1980s with a water volume balance equation and momentum equations that account for the complex rheological behavior of non-Newtonian, hyperconcentrated flows including cohesive yield stresses, Mohr-Coulomb shear stress, viscous shear stress, turbulent shear stress, and dispersive shear stress (O'Brien et al., 1993). Application of 2D models requires a digital elevation model, Manning coefficient distribution, estimates of parameters for viscous and yield stresses, and a configuration of hazard drivers such as rainfall rates and/or streamflow rates from a mountain catchment. Furthermore, 2D models output spatio-temporal distributions of flood hazards (e.g., depth and velocity) needed for exposure assessment. The entrainment of sediment into flood flows increases volumetric flow rate, a process known as bulking (Jakob et al., 2005; Meyer et al., 1995; Meyer & Wells, 1997), and acts to further magnify hazards. In practice, 2D hazard models have been applied under the assumption of a bulked flow rate defined by a bulking factor k, which represents the ratio of the volumetric flow rate of the fluid-debris mixture to the flow rate of the fluid alone, and can be linked to fire severity (Gusman, 2011). Roughly speaking, a bulking factor of 1.00–1.25 corresponds to normal streamflow, a bulking factor of 1.25–1.67 corresponds to hyperconcentrated flow, and a bulking factor of 1.67–2.86 corresponds to mud or debris flows (Gusman, 2011). These values follow definitions of debris flows as sediment-water mixtures with a sediment concentration of 50% or greater, and hyperconcentrated flows as mixtures with sediment concentrations of 20%–40% (Gusman, 2011; Pierson, 2005). 2D hazard models may assume a rigid bed (Liu & Huang, 2006; O'Brien et al., 1993) or erodible bed (Armanini et al., 2009; Li et al., 2018; Martínez-Aranda et al., 2022; Rosatti & Begnudelli, 2013). In the case of erodible bed models, an entrainment formulation is adopted to account for mass transfer from the sediment bed into the fluidized layer, and thus the bulking process is resolved. While this eliminates the need for a bulking parameter, additional parameters are typically required to resolve sediment entrainment and/or transport processes (e.g., Christen et al., 2010; Martínez-Aranda et al., 2022, and others). Whether fixed or erodible bed modeling of debris flow hazards is preferable for a particular application will depend on the availability of data to parameterize models and tolerances for uncertainties and computational costs, as erodible bed models tend to have significantly higher computational costs than rigid bed models (Majd & Sanders, 2014).

Mitigation of post-fire flood hazards has mainly been approached with two types of infrastructure: debris basins, which capture eroded coarse sediment and debris at the outlet of mountain catchments, and flood channels, which are designed to convey mixtures of runoff and fine sediment past developed areas to downstream water bodies (Jennings & Brooks, 1982; Scott & Williams, 1978). Johnson and McCuen (1992) define a debris basin as "a structure designed to contain all or part of a single debris flow or multiple debris flows for the purpose of protecting homes, roads, and property downstream of a debris-generating area." Debris basins have been used in the western United States, Japan, Europe, and Canada to mitigate hazards posed by sediment-laden flows, including debris flows (Johnson et al., 1991; Johnson & McCuen, 1992; Osanai et al., 2010; Prochaska et al., 2008; Wallerstein et al., 1997; Willardson, 2020). In general, important design parameters for sizing debris basins include the frequency of the design flow event and the magnitude of the flow (Johnson & McCuen, 1992). In southern California, design practices vary regionally depending on local regulatory bodies, but generally call for the sizing of debris basins using a combination of probabilistic precipitation intensity data and empirical models

of sediment yield that depend on watershed attributes such as slope, area, soil properties, and burn severity (Gusman, 2011). Similarly, the sizing of flood channels is based on precipitation data and semi-empirical models of peak flood discharge (Gusman, 2011).

Infrastructure is designed to meet a specific standard of performance defined by an annual return period, T, or an annual exceedance probability $p = 1/T$, and following guidelines established by county-level governments (Gusman, 2011). For example, a channel designed to contain the 20-year return period flow event has an annual exceedance probability of 5%, or smaller if a safety factor is used. The exceedance probability of a flood channel, p_c, will not necessarily be the same as the exceedance probability of the precipitation used to size it, p_p, due to compounding factors that affect the likelihood of an overtopping event (i.e., when the flow rate through the channel exceeds its flow capacity). In particular, channels are designed using specific assumptions (models) about runoff and sediment loads produced by rainfall, and assuming regular maintenance to prevent loss of flow capacity. However, the frequency and intensity of precipitation and wildfires are affected by climate change (Dennison et al., 2014; Gershunov et al., 2019; Li & Banerjee, 2021; Swain et al., 2018; Westerling et al., 2006), and sequences of storm events may lead to rapid sedimentation of debris basins and channels causing loss of channel capacity (Gusman, 2011). The lack of regular maintenance of infrastructure (e.g., removal of sediment and debris) is also a growing problem based on resource constraints (Vahedifard et al., 2017). Hence, post-fire flooding represents a compound hazard affected by both natural and human factors (e.g., Sadegh et al., 2018).

Given that the role of flood infrastructure in compound post-fire flood hazards has not previously been quantified and is poorly understood, the objective of this study is to present a new model for hazard estimation applicable to present and future compound hazards. Specifically, we are interested in estimating the exceedance probability (and associated return period) of a flood channel downstream of a mountain catchment and debris basin vulnerable to clogging with sediment. The ability to characterize compound hazards (i.e., exceedance probabilities) is important not only for improving the design of infrastructure and promoting infrastructure maintenance, but also for increasing risk awareness within affected communities (Cutter et al., 2018; Houston et al., 2019; Montz & Tobin, 2008). Moreover, improved understanding of exceedance probabilities can be paired with 2D simulations of extreme events for more effective risk communication (Luke et al., 2018; Sanders et al., 2020). Two specific questions about post-fire flood hazards will be addressed herein:

1. How does the frequency of channel exceedances vary in areas exposed to post-fire compound flood hazards based on current design standards and maintenance approaches?
2. How will the frequency of channel exceedances change in the future based on increasing fire frequency and fire severity?

The remainder of the study is organized as follows: Section 2 (Methods) presents the conceptual model and stochastic methods for capturing the interdependence between wildfires, rainfall, infrastructure sedimentation, and flooding. Section 3 (Results) shows the estimation of hazards for a range of fire frequencies and severities, infrastructure design standards, and maintenance approaches. Section 4 (Discussion) contrasts the return period of channels due to the compound hazard versus those of the precipitation used for design due to the marginal hazard, and contemplates the implications for risk management. Section 5 presents conclusions.

2. Methods

2.1. Model Overview

We apply Monte Carlo (MC) methods to simulate the compound hazard (Kroese et al., 2014). MC methods provide a robust approach for characterizing the uncertainty inherent in estimates of compound hazards linked to the variability in the random variables that drive them–in this case, wildfire and precipitation. They can also be used to generalize complex models of physical systems into a set of basic events and interactions that is simpler, more computationally efficient, and more scalable than a model produced by analytic methods (Kroese et al., 2014). Unlike deterministic approaches to modeling hydrologic processes, stochastic approaches like MC methods allow modelers to use a single record of precipitation or floods to forecast a range of statistically possible futures for a given watershed, enabling a much richer understanding of future hydrologic conditions and evaluation of flood infrastructure (Vogel, 2017). Stochastic modeling approaches are preferable to deterministic ones when evaluating the implementation of different management alternatives because the former can determine whether a difference in outcomes between alternatives is significant in a statistical sense, while the latter can only

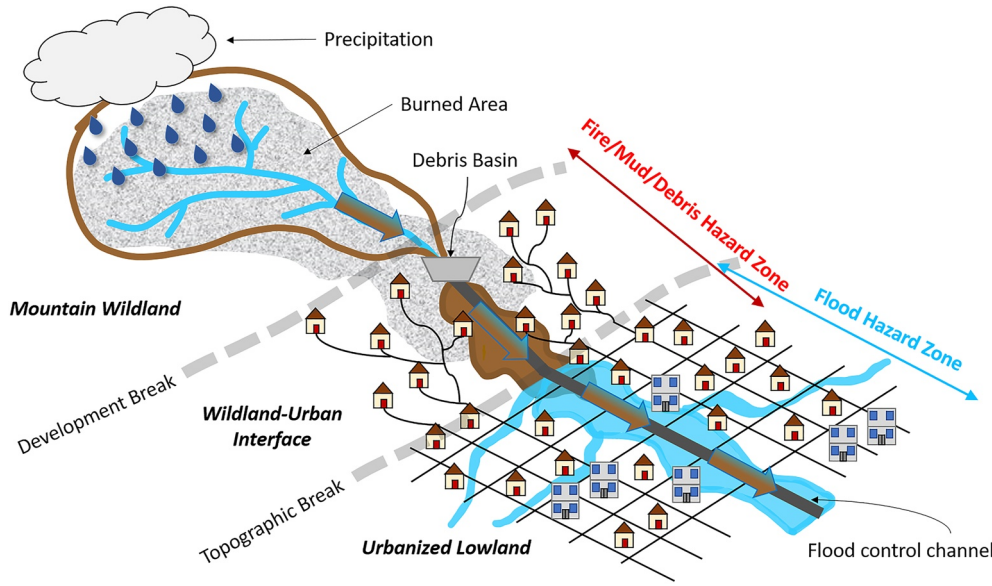

Figure 1. Conceptual diagram of the development of post-fire flood and debris flow hazards due to infrastructure clogging.

provide a single estimate indicating whether the outcomes differ. Moreover, stochastic modeling is valuable for estimating the probability that a particular management or design alternative achieves a specific goal, which is particularly useful information for flood management (Brand et al., 2020).

We consider a mountain watershed with a set of properties, **p**, that control the volumetric flow rate of clear streamflow, Q, and sediment, J, in response to precipitation, P. Elements of **p** may include various factors such as watershed morphology, soil properties, vegetative cover, or burn severity, and precipitation can be interpreted in various ways (e.g., hourly and daily). For the moment, we leave this in a general form so the derivation herein is most easily transferred between systems and poised to leverage the best available information on a site-by-site basis. Hence, we write streamflow and sediment flux at the watershed scale as follows.

$$Q_{\mathrm{w}} = f_Q(\mathbf{p}, P) \tag{1}$$

$$J_{\mathrm{w}} = f_J(\mathbf{p}, P) \tag{2}$$

where the subscript w denotes *watershed* and the functions $f_Q()$ and $f_J()$ characterize peak streamflow and peak sediment fluxes, respectively. For this study, we use the Rational Method to compute Q_{w} as follows,

$$Q_{\mathrm{w}} = \frac{cPA}{t_{\mathrm{p}}} \tag{3}$$

where c is a dimensionless runoff coefficient representing the ratio of rainfall to surface runoff, P is the daily rainfall accumulation, A is the watershed area, and t_{p} is a time scale representing the time to peak of a triangular hydrograph. We note that model dependency on geomorphological parameters will depend on the choice rainfall-runoff models (e.g., Chen et al., 2013; Goodrich et al., 2012; Kinoshita et al., 2014).

The total sediment volume associated with a storm event can be written in a general way as follows,

$$V_{\mathrm{w}} = \int_0^{t_{\mathrm{s}}} J_{\mathrm{w}}\, dt \tag{4}$$

where t_{s} represents the storm duration.

Debris basins are located at the outlets of mountain watersheds to capture coarse sediment and debris and prevent the clogging of downstream flood control channels, which are designed to convey only water and small amounts of fine sediment past developed areas into a downstream water body (Figure 1). The debris basins fill with eroded sediment during storms, especially those after fires, and are typically emptied during dry weather periods through

excavation. If a debris basin fills completely, sediment fluxes bypass the debris basin and flow into a downstream flood channel where flow capacity is reduced through clogging, the settling out of sediment as the flow slows down, and increased flow resistance. The volume of sediment in a debris basin, $\forall_b$, can be modeled based on mass conservation as follows,

$$\frac{d\forall_b}{dt} = J_w - J_c - J_e \tag{5}$$

where J_c represents the volumetric flux of sediment flowing out of the debris basin and into the flood *channel*, and J_e represents the flux of sediment removed from the debris basin by *excavation*. The sediment flux from the debris basin into the flood channel is assumed to be zero when debris basin storage is below capacity and equal to the inflow rate otherwise,

$$J_c = \begin{cases} 0 & \text{if } \forall_b < \forall_b^{des} \\ J_w & \text{otherwise} \end{cases} \tag{6}$$

where $\forall_b^{des}$ represents the *design* capacity of the debris basin. The excavation flux is driven by human activity and generally occurs episodically between precipitation events. For example, excavation may occur over several days to weeks during dry weather periods once the infrastructure has filled to a cleaning threshold (e.g., 85% full), subject to various constraints such as the availability of funding, wetland protection policies, and the Endangered Species Act (RCFCWCD, 2021). J_e can thus be considered a function that is prescribed to vary over time depending on local maintenance practices. Additional details on the implementation of maintenance protocols within the model are provided in Section 2.5.

If the debris basin attenuates the flood peak, then the peak flow rate entering the channel can be expressed as a fraction of the peak flow from the watershed,

$$Q_c = \alpha_b Q_w \tag{7}$$

although in many cases the debris basin will not be designed to attenuate the flood peak and thus $\alpha_b = 1$.

The bulked flow of water and sediment, a simple sum of Equations 1 and 2, has been previously introduced for sizing infrastructure and quantifying hazards in areas impacted by mud and debris flows and appears as follows,

$$B = Q + J = kQ \tag{8}$$

where k represents a bulking factor expressed as follows,

$$k = \frac{Q + J}{Q} = \frac{1}{1 - \frac{c_v}{100}} \tag{9}$$

where c_v represents the percentage concentration of sediment by volume in the bulked flow. Streamflow in small watersheds and alluvial fans is typically characterized by a bulking factor of 1.25 or less (1.0 corresponds to clear water), but after burn events, watersheds may produce hyperconcentrated flows with a bulking factor of up to 1.67 or mud and debris flows with a bulking factor of 2.0 or greater (Gusman, 2011). The magnitude of the bulking factor, k, is varied over time to represent the effects of the occurrence and severity of wildfires on watershed hydrology, as described in detail in Section 2.2.

Flood hazards downstream of mountain watersheds occur when the bulked flow rate into the flood channel, B_c, exceeds the channel capacity (more information on how channel design capacities are typically determined can be found in Section 2.4). While flood channels are designed to accommodate a peak discharge associated with a storm or flood of a certain return period, over time they may fill with sediment and may also grow vegetation that reduces channel capacity. Consequently, channel capacity, is assumed to decrease with sedimentation as follows,

$$D_c^{\text{eff}} = \begin{cases} D_c^{\text{des}} \left(1 - \frac{\forall_c}{\forall_c^{\text{des}}}\right) & \text{if } \frac{\forall_c}{\forall_c^{\text{des}}} < 1 \\ 0 & \text{otherwise} \end{cases} \tag{10}$$

where D_c^{des} is the design capacity of the channel, $\forall_c$ is the volume of sediment in the channel and $\forall_c^{\text{des}}$ is the design volume of the channel. Now that both the bulked flow rate in the channel and the channel capacity are established, the flood hazard, H, is given by the exceedance of channel flow over capacity as follows,

$$H = \begin{cases} B_c - D_c^{\text{eff}} & \text{if } B_c > D_c^{\text{eff}} \\ 0 & \text{otherwise} \end{cases} \tag{11}$$

The above formulation captures the interdependence between wildfires, precipitation, infrastructure sedimentation and hazards, and is poised to inform research into the ways in which flood hazards are impacted by changes in fires, rainfall, infrastructure design, and infrastructure maintenance. Several modes of interdependence are captured by the model as follows: First, wildfires alter watershed properties, **p**, that increase the bulk discharge (Equation 8) through increases in the clear water flux (Equation 1) and sediment fluxes (Equation 2). Second, bulked flows that cannot be contained by debris basins reduce the capacity of flood channels (Equation 10) and lower the threshold for channel bank overtopping (Equation 11). And third, the capacity of debris basins and channels is impacted by excavation and cleaning schedules, which in turn are impacted by available funding and various environmental constraints (Section 2.5).

2.2. Wildfire Occurrence and Severity Models

The bulking factor, k, is used to quantify the effect of wildfire on streamflow and sediment flux as a function of the time elapsed since the fire occurred. Multidecadal records of sediment production and streamflow from the San Gabriel Mountains of southern California show that the effect of wildfire on erosion and runoff is greatest immediately following the fire, which strips hillslopes of vegetation and may alter surficial soil properties, and decays exponentially during the first 5 years following fire as vegetation and surficial soils recover (Lavé & Burbank, 2004). Studies of sediment yields in the Transverse Ranges of southern California have used a similar exponential decay function termed a "lingering effect" to model the decreasing influence of wildfire on sediment production over time as watershed vegetation recovers; in these studies, the decay constant has been varied to represent a recovery time (i.e., time to return to pre-fire conditions) of 2–10 years (Gartner et al., 2009, 2014). Hence, the occurrence of a wildfire is represented by an increase in the bulking factor from a pre-fire, baseline level, k_0, to a post-fire level, k_1. Following the start of the fire, the bulking factor decays exponentially according an adjustable parameter termed the "recovery timescale" of the watershed, t_r, as follows,

$$k(t) = k_0 + (k_1 - k_0)\, e^{-t/t_r} \tag{12}$$

where t is the number of days elapsed since the start of the wildfire. Once the bulking factor falls within 1% of k_0, the watershed is no longer considered to be actively burned, and $k(t) = k_0$ until the next fire occurs. Thus, the recovery time of the watershed following a given fire will depend on the value of the post-fire bulking factor, k_1, which is taken to be a proxy for the severity of the fire. The greater the k_1, the longer it will take for the bulking factor to return to its baseline level, k_0. For each wildfire, k_1 is simulated stochastically following Equation 14 below.

Fire occurrence is modeled using an MC method that makes use of the probability that a fire will occur on a given day during the fire season, p_f. This daily exceedance probability is modeled as a Bernoulli random variable as follows,

$$p_f = 1 - \left(1 - \frac{1}{T_f}\right)^{1/n} \tag{13}$$

where T_f is the annual fire interval and n is the number of days in the fire season. The parameter T_f is adjustable and can be changed to simulate the effect of different historical or projected fire frequencies on post-fire flood hazards. On each day of the fire season, the output from a uniform random number generator, $u \sim U(0, 1)$, is compared to p_f. If $u < p_f$, an active burn is initiated and the bulking factor for that day is set to k_1. Thereafter, the magnitude of the bulking factor will decay exponentially according to Equation 12 until it is within 1% of the pre-fire bulking factor, at which point it will be reset to k_0. Otherwise, if $u \geq p_f$, then $k(t) = k_0$.

In this study, fire occurrence is limited to the months of July to August ($n = 62$) according to the peak fire season in California (Li & Banerjee, 2021), but can be adjusted based on the fire season of any region or to simulate different climate change scenarios. We consider fire intervals of 50, 20, 15, 10, 5, and 2 years based on a map of fire intervals for major vegetation types in California from 1908 to 2012, which shows that the range of fire intervals for mountain watersheds in southern California spans from 7 to 52 years (USDA Forest Service, 2012). We include the 2-year and 5-year fire interval scenarios to represent possible futures in which wildfire frequency has increased relative to historical levels. Note that the selection of the 2-year and 5-year fire intervals is not based on specific predictions of future wildfire frequency in the region, but rather is intended to illustrate the sensitivity of post-fire flood hazards to hypothetical increases in fire frequency. In an effort to avoid an overly complex model of the effect of wildfire on watershed hydrology, only one active burn can be simulated at a time, which is a reasonable assumption at the watershed scale since a wildfire consumes fuel, and another wildfire is unlikely to occur in the same area while the watershed is recovering (Moody et al., 2013).

Given the considerable natural variability in fire intensity and thus burn severity of wildfires that may occur within a watershed over time, the post-fire bulking factor, k_1, is modeled as a uniformly distributed random variable with a specified range as follows,

$$k_1 = k_1^{\min} + \left(k_1^{\max} - k_1^{\min}\right) v \tag{14}$$

where $k_1^{\min}$ and $k_1^{\max}$ are the lower and upper limits of the range, respectively, and $v \sim U(0, 1)$. We use a uniform random distribution since no prior information is known about the distribution of post-fire bulking factors, and thus assign probabilities equally to all possible bulking factors within the specified range. The limits of the post-fire bulking factor range can be selected based on the range of observed sediment fluxes from a given watershed or to represent the effect of different burn severities on post-fire sediment fluxes. We assume that the post-fire bulking factor increases with increasing burn severity, an assumption supported by studies that found increasing sediment fluxes with increasing burn severity class (Cannon et al., 2010; Gartner et al., 2014; D. Vieira et al., 2015).

By representing wildfire occurrence and severity as stochastic processes, many scenarios of varying fire frequencies and severities can be simulated and the potential effects of wildfire characteristics on post-fire flood hazards are more thoroughly explored. For this study, k_1 was uniformly sampled from a range representing the severity of a fire as follows:

1. Low burn severity: $1.10 < k_1 < 1.25$
2. Moderate burn severity: $1.25 < k_1 < 1.67$
3. High burn severity: $1.67 < k_1 < 2.86$

We chose these ranges for each burn severity class because they roughly demarcate transitions in flow types between normal streamflow, hyperconcentrated flow, and mud flows and debris flows (Gusman, 2011).

2.3. Precipitation Model

Following Wilks (1998), precipitation was simulated as a stochastic process using a first-order Markov chain to describe precipitation occurrence and MC sampling from an appropriate probability distribution to describe precipitation amounts for days with rain (e.g., Richardson, 1981; Stern & Coe, 1984). The Monte Carlo Markov Chain (MCMC) rainfall simulator was developed using a long-term daily precipitation record (1932–2020) from the Big Tujunga Dam station in Los Angeles, California (ID: USC00040798) retrieved from the Climate Data Online database maintained by the U.S. National Oceanic and Atmospheric Administration (NOAA, n.d). This meteorological station was chosen for its length of record and its location at high elevation in the San Gabriel Mountains, since watersheds prone to post-fire flood hazards tend to be mountainous.

To preserve the distribution of wet versus dry years present in the long-term precipitation data set, we divided the data into subsets for wet years ($N = 27$ years) and dry years ($N = 44$ years), where "wet years" were defined as those with total annual precipitation greater than or equal to the mean. Years missing 10% or more daily values were excluded from the analysis. We used the wet-year and dry-year designations to calculate the conditional probability of transitioning from a dry year to a wet year, p_{DW}, and from a wet year to a wet year, p_{WW}. This was done by counting the number of transitions for each possible type of transition: dry-to-wet (DW), dry-to-dry (DD), wet-to-dry (WD), and wet-to-wet (WW). Then the annual transition probabilities were calculated as follows.

$$p_{DD} = \frac{F_{DD}}{N_D} \tag{15}$$

$$p_{DW} = 1 - p_{DD} \tag{16}$$

$$p_{WW} = \frac{F_{WW}}{N_W} \tag{17}$$

where F represents the number of times a transition occurred and N represents the number of wet or dry years on record (Adane et al., 2020; Shahraki et al., 2013; Sumeet et al., 2013).

Modeling daily precipitation occurrence as a first-order Markov process assumes that the probability of observing precipitation on a given day depends only on whether precipitation occurred the previous day, regardless of whether precipitation occurred on earlier days in the time series. We define a "wet day" as a day on which at least the minimum reportable precipitation amount occurred, 0.254 mm. The parameters p_{01} and p_{11} represent the conditional probability of transitioning from a dry day to a wet day and transitioning from a wet day to a wet day, respectively. These daily transition probabilities were estimated from the wet-year and dry-year subsets separately by grouping the data by ordinal day (1–365, where 365 represents December 31 of a non-leap year) and performing the same calculations in Equations 15–17 on a daily time scale. Again, years missing 10% or more daily values were excluded from the analysis. Average daily transition probabilities were calculated using a 14-day moving average of the empirical probabilities to smooth extreme values (Figure S1 in Supporting Information S1).

The MCMC rainfall simulator generates $m \times 365$ days of a daily precipitation time series, where m is the number of years in the time series, as follows: for the first year of the time series, a random number is generated to determine the wet or dry status of the first year, with a 50% chance for either outcome. The appropriate wet-year or dry-year daily transition probabilities are then used to simulate 1 year of a daily precipitation time series. This is done by generating a random number to determine the wet/dry status of the first day in the time series, which in turn determines the "threshold transition probability," p_t, that will be used to predict the wet/dry status of the next day. The threshold transition probability for day t is given by,

$$p_t = \begin{cases} p_{01} & \text{if } X_{t-1} = 0 \\ p_{11} & \text{if } X_{t-1} = 1 \end{cases} \tag{18}$$

For each day of the year, p_t is compared to the output from a uniform random number generator, $u_t \sim U(0, 1)$. Rainfall occurrence on day t is then calculated as follows,

$$X_t = \begin{cases} 1 & \text{if } u_t \le p_t \\ 0 & \text{otherwise} \end{cases} \tag{19}$$

The precipitation amount for each wet day is determined by randomly sampling from a Weibull distribution fit to the observed non-zero precipitation amounts from wet years and dry years separately. The Weibull distribution was selected after comparing the fit of four probability distributions commonly used for non-zero rainfall amounts in the literature (e.g., Sharma & Singh, 2010; F. M. C. Vieira et al., 2018; Ye et al., 2018). Goodness of fit was assessed with a comparison of quantile-quantile (Q-Q) plots between the fitted probability distributions

(Figure S2 in Supporting Information S1) and Q-Q plots of the wet-year and dry-year subsets versus the fitted Weibull distribution (Figure S3 in Supporting Information S1).

The wet/dry status of the next year in the time series is determined in a similar manner to that shown in Equations 18 and 19, except the annual transition probabilities, p_{DW} and p_{WW}, are used.

2.4. Infrastructure Design Standards

In southern California, due to the frequency of post-fire flood events, many flood control agencies estimate bulking factors or sediment yields for watersheds that produce high levels of sediment, burn frequently, or are located upstream of critical infrastructure, such as hospitals or transportation infrastructure (Gusman, 2011). Bulking factors are applied as a safety factor to the peak discharge used to design flood control channels, while sediment yields are estimated to determine the design capacity of debris basins. The specific equations and procedures used to determine design bulking factors and sediment yields vary widely from county to county, but in general they involve a design storm of a certain return level, which is translated into a design peak discharge using a rainfall-runoff relationship. Two counties in particular, Los Angeles and Ventura County, provided detailed descriptions of the design standards for debris basins and flood channels in design manuals (LACDPW, 2006a; 2006b; VCWPD, 2005, 2017). Specifically, Los Angeles County requires all debris basins to be designed for a 50-year design storm (termed the "Capital Flood"), and the sediment yield for a "design debris event" is determined using curves calculated for each "debris producing area" in the county based on watershed area and an assumption of 4 years since the watershed was last burned. Bulking factor curves are used to calculate bulking factors used to design flood channels in sediment producing watersheds where a debris basin does not exist (LACDPW, 2006b). Ventura County, on the other hand, requires debris basins for watersheds with areas <5 mi^2 to be designed to hold 125% of the sediment volume expected from a 100-year design storm, provided sufficient land is available. The design sediment yield is determined using a regression equation that takes into account the watershed area and morphology, as well as a dimensionless "fire factor" that represents the percentage of non-recovery of a watershed following a burn; normal (i.e., non-emergency) design conditions assume 4.5 years since the watershed was last burned. It should be noted that the Ventura County Debris Basin Manual states, "A number of the debris basins do not have sufficient storage for the 100-year debris yield and therefore could possibly fill with sediment during extreme storm events" (VCWPD, 2005). Bulking factors are applied to the design of flood channels downstream of watersheds known to produce high levels of sediment or experience frequent fires as well as those designed to protect critical infrastructure shortly after a fire (VCWPD, 2017).

The two key design criteria implemented in the model to represent regional differences in infrastructure design standards are the precipitation of the design storm, P^{des}, and the decision whether to use a clear-water or a bulked peak discharge as the design discharge. In the model presented here, P^{des} is determined by performing an extreme value analysis on a 100-year precipitation time series generated by the MCMC rainfall simulator. A Generalized Extreme Value distribution was fit to the 100-year time series of annual maximum precipitation to determine the magnitudes of the 50-year and the 100-year design storms (Figure S4 in Supporting Information S1). Next, the peak discharge associated with the return level of the design storm is calculated using the Rational Method as follows,

$$Q_w^{peak} = \frac{c P^{des} A}{t_p} \tag{20}$$

where Q_w^{peak} is the peak clear-water discharge from the watershed, c is a dimensionless runoff coefficient, A is the watershed area, and t_p is a time scale representing the time to peak of a triangular hydrograph. Note, however, that any rainfall-runoff model may be used to calculate Q_w^{peak}.

The design discharge may be calculated as either a clear-water or a bulked volumetric flow rate. If the bulked design discharge is used, a design bulking factor, k_{des}, will be applied to the clear-water discharge, Q_w^{peak}, to determine the design capacity of the flood control channel. Otherwise, the channel design capacity is set equal to Q_w^{peak}. Similarly, the capacity of the debris basin also depends on the design storm return period and whether bulking is applied to the flow from the watershed. Based on a clear-water design standard or a bulked design standard, the capacity of the debris basin is calculated as follows,

$$V_b^{des} = \begin{cases} 0.15 \times c P^{des} A & \text{clear-water standard} \\ (k_{des} - 1)\, c P^{des} A & \text{bulked standard} \end{cases} \quad (21)$$

assuming that the concentration of sediment in normal streamflow within an alluvial fan is typically at most 15% by volume (Gusman, 2011). Note that the use of the 15% sediment concentration is not a safety factor, but rather an approximation of the typical sediment flux expected from an unburned watershed used to determine the design capacity of the debris basin assuming a clear-water design standard.

In the present study, we compare four sets of infrastructure design standards generalized from the design approaches described above:

1. 50C: 50-year design storm ($p_p = 0.02$), clear-water design discharge
2. 50B: 50-year design storm ($p_p = 0.02$), bulked design discharge
3. 100C: 100-year design storm ($p_p = 0.01$), clear-water design discharge
4. 100B: 100-year design storm ($p_p = 0.01$), bulked design discharge

It is important to note that by including a clear-water design discharge, we do not imply that such a design standard is operationally applied to watersheds that are known to burn frequently or produce high levels of sediment. Rather, it is included to provide a conceptual contrast to the effects on the flood hazard of bulking the design discharge. Including a clear-water design standard also allows the exploration of what might happen if a watershed not previously identified as fire-prone was burned and its infrastructure was not designed to convey significantly bulked flows.

Finally, we note that the flood infrastructure design standards described herein are representative of debris basin design globally, in that the capacity of the infrastructure is determined based on the magnitude of an event with a particular (design) return period (Johnson et al., 1991; Johnson & McCuen, 1992; Osanai et al., 2010). We acknowledge, however, that differences in designs can be expected based on differences in equations for frequency analysis and the estimation of (post-fire) flow rates.

2.5. Infrastructure Maintenance Models

One example of a typical maintenance schedule for debris basins in Riverside County is annual inspection during the summer months to determine maintenance needs; if the cleaning threshold is met or exceeded, the debris basin will be returned to 100% capacity. In a year during which a major fire has occurred, the capacity of debris basins is restored or sometimes enhanced beyond 100% (i.e., with excavation beyond the initial grading of the basin) as soon as possible following fire containment. While excavation of debris basins can occur during the wet season, it is avoided by flood control agencies when possible because wet sediment is difficult to excavate, costly to move, and may not be accepted at the ultimate location of disposal. The excavation rate varies depending on how urgently the need for cleaning is, that is, how close the debris basin is to overfilling, with faster cleaning rates and higher maintenance costs the closer the capacity is to 0% (RCFCWCD, 2021).

These maintenance protocols have been generalized and implemented as four maintenance approaches:

1. S: Summer Cleaning
2. SA: Summer + After-fire Cleaning
3. SAW7: Summer + After-fire + Wet Season Cleaning with 7-day waiting period
4. SAW1: Summer + After-fire + Wet Season Cleaning with 1-day waiting period

When the Summer Cleaning model is active, the levels of sediment in the debris basin and the flood channel are checked each day during the summer months (June 1 to September 29); if the level of sediment in a given facility is greater than or equal to the cleaning threshold, the facility will be "excavated" and returned to full capacity.

When the After-fire Cleaning model is active, if a fire occurred during a given year, the debris basin will be "excavated" on September 30, the nominal last day of the summer, and returned to full capacity.

Finally, when the Wet Season Cleaning model is active, the level of sediment in the debris basin is checked each day during the wet season (October 1 to April 30); if the level of sediment in the debris basin is greater than or

equal to the cleaning threshold *and* if a certain number of days have passed without rain, the debris basin will be "excavated" at a certain cleaning rate (volume of sediment per day). The "waiting period" between storms and cleaning rate are used to represent the effort to incrementally excavate sediment during dry periods between storms in the wet season; both parameters can be estimated from debris basin cleaning records.

2.6. Model Summary and Limitations

The framework developed herein for hazard simulation can be considered a lumped system dynamics model for estimating exceedance probabilities in channel reaches downstream of debris basins and upstream of confluences from other streams. Key physical elements of the framework include the watershed, debris basin, and flood channel as shown in Figure 1, and the key state variables include the bulking factor, debris basin storage of sediment, channel storage of sediment, daily precipitation accumulation, daily sediment fluxes, and flood peaks accounting for water and sediment fractions. Each of these state variables represents approximations of processes that could be subject to more refined modeling. In particular, the generation of runoff and entrainment of solids from hillslopes and channels involves many different physical processes active at a range of spatial and temporal scales (Jakob et al., 2005; Moody et al., 2013; Shakesby, 2011). It should be noted that while unit-area runoff and sediment fluxes are generally expected to decrease with increasing contributing area in semiarid regions (e.g., Mayor et al., 2011; Nadal-Romero et al., 2011; Wagenbrenner & Robichaud, 2014), the model as currently configured estimates that these variables are insensitive to changes in watershed area (Figure S5 in Supporting Information S1). This is a consequence of calculating clear-water runoff from the watershed (Q_w) using the Rational Method (Equation 3) and sediment flux from the watershed (J_w) as a linear function of Q_w and the bulking factor, k. Additionally, the clogging of channels may result from complex interactions between channel geometry, channel vegetation, hydraulic structures, and the flow regime such as whether and to what extent the flow entrains large woody vegetation, mud, and rocks (Luke et al., 2018; Piton & Recking, 2016; Rickenmann et al., 2006). Finally, the probability of wildfire occurrence and the severity of a given wildfire depend on several factors including the availability and composition of fuel, climatic controls such as humidity, and the topography of the landscape (Finney, 2005; Littell et al., 2016). In this light, stochastic modeling approaches are advantageous because uncertainty can be captured with random variables that span a range of possible values, as we have done for the bulking factor.

2.7. Hazard Simulations

Results are organized into two sets of simulation scenarios: Model Illustration Scenarios and Stochastic Hazard Scenarios. The Model Illustration Scenarios demonstrate how the framework estimates compound post-fire flood hazards under three infrastructure management scenarios using 100-year stochastic simulations that account for the combined effects of wildfires, rainfall, infrastructure design, and maintenance. The Stochastic Hazard Scenarios consist of four sets of scenarios used to systematically investigate post-fire flood hazards in relation to four separate factors: infrastructure design standard, infrastructure maintenance approach, fire interval, and fire severity. The model settings for each simulation scenario are shown in Table 1.

The model parameters that were not varied within a given simulation scenario were kept constant between the different scenarios to ensure a fair comparison. The baseline parameter values used in this study were chosen to simulate a representative watershed system and flood infrastructure system in southern California and are displayed in Table 2. The same synthetic precipitation time series was used in each simulation (displayed in Figure 2a) for consistency across results.

2.8. Model Outputs

For each scenario, a total of 3,000 MC trials were simulated, each trial yielding a 100-year daily time series of peak channel flows and channel capacities from which the number of years per century with at least one channel exceedance, n_c, was computed. The annual exceedance probability, p_c, was computed for each MC trial empirically as follows,

$$p_c = n_c/100 \tag{22}$$

Table 1
Simulation Scenarios

	Scenario name	Model settings[a]	Model output	Figure
Model Illustration Scenarios	Scenario 1: Low Protection	50C, S	Overbank flows (m^3/s)	2
	Scenario 2: Moderate Protection	50B, S		
	Scenario 3: High Protection	50B, SAW1		
Stochastic Hazard Scenarios	Design Standards and Fire Interval	50C, 100C, 50B, 100B 50, 20, 15, 10, 5, 2 (years)	Empirical flood return period (years)	3
	Maintenance Approach and Fire Interval	S, SA, SAW7, SAW1	1. Empirical flood return period (years)	4
		50, 20, 15, 10, 5, 2 (years)	2. Sediment excavated from infrastructure (m^3)	5
	Design Standards and Burn Severity	50C, 100C, 50B, 100B $1.10 < k_1 < 1.25$, $1.25 < k_1 < 1.67$, $1.67 < k_1 < 2.86$	Empirical flood return period (years)	6
	Maintenance Approach and Burn Severity	S, SA, SAW7, SAW1 $1.10 < k_1 < 1.25$, $1.25 < k_1 < 1.67$, $1.67 < k_1 < 2.86$	Empirical flood return period (years)	7

[a]Abbreviations are defined in Sections 2.2, 2.4, and 2.5.

and a flood return period, T_c, follows as,

$$T_c = 1/p_c \quad \text{for} \quad p_c > 0 \tag{23}$$

The progression of MC trials yields distributions of T_c values that are examined to infer dependencies on infrastructure design standards, infrastructure maintenance approaches, fire interval, and wildfire severity. Distributions are presented by combining box plots and violin plots. Box plots are displayed as follows: widths are

Table 2
Baseline Model Parameters

Variable/parameter	Value	Rationale
Watershed area, A	3 km^2	Average area of watershed in southern California (Gartner et al., 2014)
Pre-fire bulking factor, k_0	1.00	Corresponds to clear streamflow
Post-fire bulking factor, k_1	1.25–2.86	Represents a range of flow types from hyperconcentrated flow to debris flows
Fire interval, t_f	20 years	Roughly representative of southern California (USDA Forest Service, 2012)
Design standard	50B	Represents standard used by Los Angeles County, which has set precedents in the estimation of design bulking factors for the region (Gusman, 2011)
Design bulking factor, k_{des}	1.20	Based on past studies by the Ventura County Watershed Protection District (VCWPD, 2017)
Maintenance approach	S	A commonly used approach in southern California (RCFCWCD, 2021)
Infrastructure cleaning threshold	85% filled	Based on correspondence with Riverside County (RCFCWCD, 2021)
Debris basin cleaning rate	1,800 m^3/day	Based on debris basin excavation records provided by Riverside County
Watershed recovery timescale, t_r	365 days	Assumes recovery time of 5 years following debris flow event (Lavé & Burbank, 2004)
Runoff coefficient, c	0.3	Used to calculate Q_w; based on commonly used values for natural land use types with >6% slope

10.1029/2022EF002670

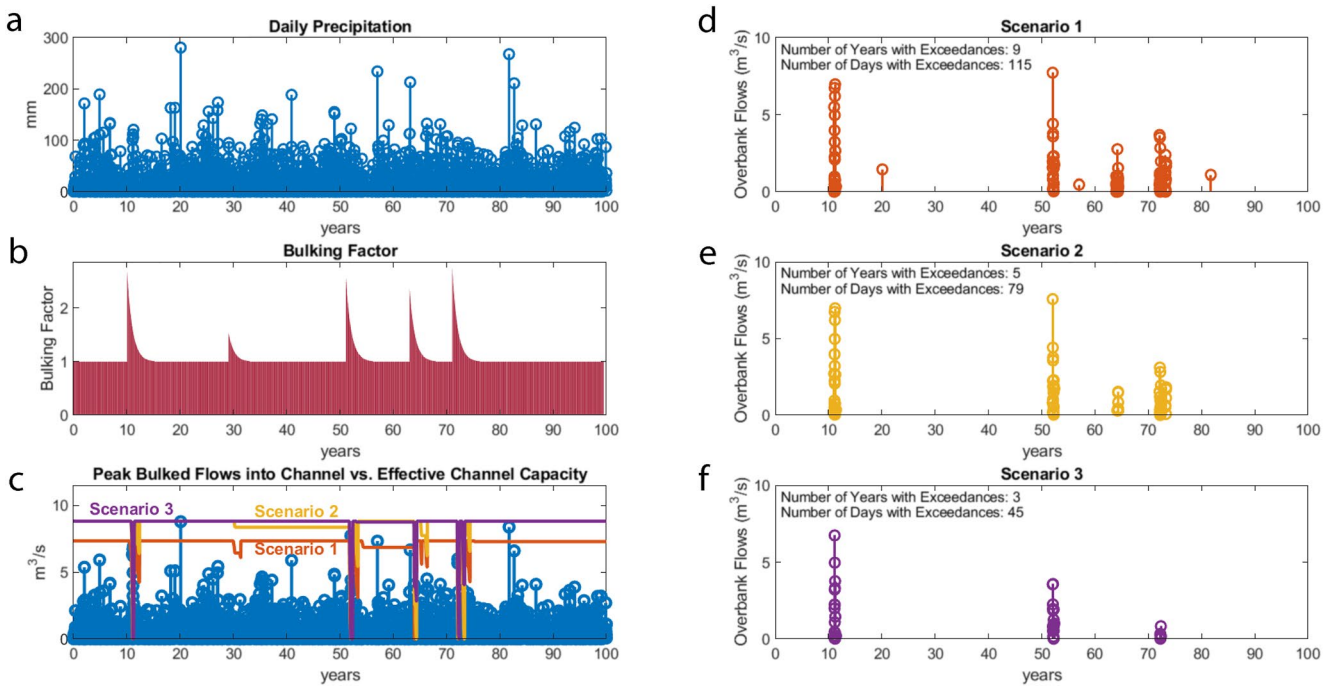

Figure 2. Time series of (a) daily precipitation, (b) bulking factor, (c) peak bulked flows from the debris basin into the channel and (d–f) the corresponding time series of overbank flood flows for three management scenarios. Management scenarios are defined in Table 1. The effective flood channel capacity time series for the three scenarios are compared in panel (c).

proportional to the square root of the sample size for each scenario; the central line corresponds to the median and the lower and upper edges correspond to the first and third quartiles, respectively; the upper whisker is calculated as min(max(x), Q3 + 1.5 × IQR); the lower whisker is calculated as max(min(x), Q1 1.5 × IQR); and outliers are not displayed. For the violin plots, Gaussian kernel smoothing was used.

We note that a "No Fires" scenario was also considered as a check on numerical consistency. In the absence of wildfire, the compound hazard reverts to the marginal hazard scenario (precipitation and runoff in the absence of wildfire), and the channel return period matches the precipitation return period, $T_c = T_p$. In all cases, the computed median value of T_c from 3,000 MC simulations was found to match the return period (either 50-year or 100-year) of the precipitation return level used for runoff modeling, peak discharge estimation (Equation 1), and sizing of channels according to the clear-water design standard.

3. Results

3.1. Illustration of Compound Post-Fire Flood Hazard Estimation

The simulation begins with a 100-year stochastic time series of daily precipitation (Figure 2a), the bulking factor (Figure 2b), and daily peak bulked flows into flood channels (Figure 2c, blue stem plot). Note that the simulation includes five fire events with different peak bulking factors, which correspond to random numbers, and that the bulking factor exponentially decays back to a baseline value of unity for several years after each fire event. The filling of infrastructure with sediment is sensitive to the management scenario (Scenario 1, 2, or 3), which in turn impacts the capacity of the flood channel (Figure 2c, orange, yellow, and purple lines, respectively) and the number of days when peak bulked flows exceed channel capacity (Figures 2d–2f, respectively).

Hazards can be estimated based on the number of years or days with exceedances of the channel capacity. Figures 2d–2f show that with increasingly conservative flood management approaches (Scenario 1, 2, and 3, respectively), the number of years with exceedances of channel capacity is reduced (9, 5, and 3 out of 100) and the number of days with exceedances is reduced (115, 79, and 45 over 100 years).

10.1029/2022EF002670

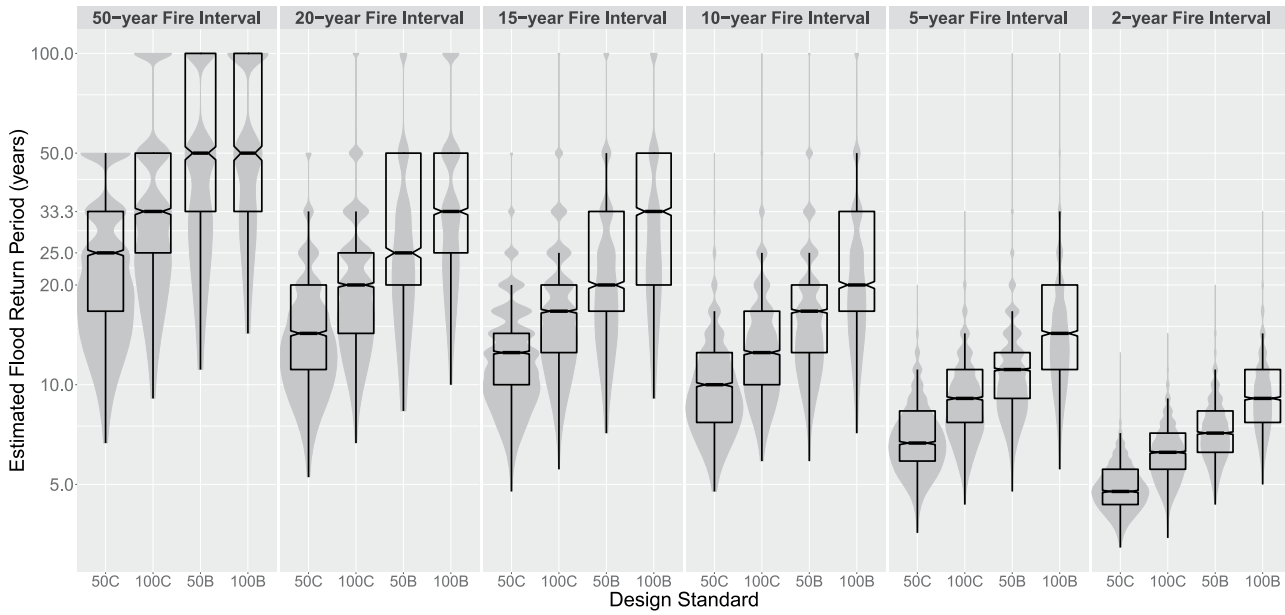

Figure 3. Simulated distributions of flood return period versus infrastructure design standard (50C, 50B, 100C, and 100B) and fire interval.

An important dynamic captured by the simulation framework is the coincidence of high bulking factors and high peak precipitation, which leads to high peak bulked flows. For example, following a fire event in Year 10 that yields a bulking factor exceeding 2.0, overtopping events are predicted across all three management scenarios with rainfall less than 150 mm/day; on the other hand, rainfall of nearly 300 mm/day in Year 20 only yields a small rate of overtopping in Scenario 1, while no flooding is predicted under Scenarios 2 and 3.

3.2. Flood and Debris Hazards Versus Fire Interval

Figure 3 shows T_c distributions across four different *infrastructure design standards* (50C, 100C, 50B, and 100B) and six different *fire intervals* (50-year, 20-year, 15-year, 10-year, 5-year, and 2-year). Return period is expected to decrease below that of the precipitation design level (50 or 100 years) with wildfires that alter runoff and sediment production, and Figure 3 shows the rates of decrease with decreasing fire intervals. Notably, median flood return period was computed to be 2–10.5 times smaller than expected based on a 50-year design standard and 3–16 times smaller than expected based on a 100-year design standard. For example, infrastructure designed based on a 50-year design storm assuming clear-water discharge (50C) delivers protection corresponding only to a 10-year return period when the fire interval is 10 years. Further, infrastructure designs that take a more conservative approach, such as a 100-year design storm assuming a bulked discharge (100B), only offer protection corresponding to a 20-year return period when the fire interval is 10 years. The most conservative design scenario (100B) produces a median flood return period that is 1.8 times larger than that of the least conservative design scenario (50C), across all fire frequencies.

Figure 4 shows T_c distributions across four different *maintenance approaches* (S, SA, SAW7, and SAW1) based on the same fire intervals as before and infrastructure designed based on a 50-year storm and a bulked discharge (50B). The comparison of the flood return period distributions shows that differing maintenance approaches play a major role in moderating risks. For example, the most conservative maintenance scenario (SAW1) produces a median flood return period that is twice as large as that of the least conservative maintenance scenario (S).

Sediment management costs tend to vary based on a number of factors such as sediment size distribution, presence of contaminants, challenges with access, level of moisture, and access to a disposal site (Brand et al., 2020), but a controlling consideration is the volume of material that needs to be removed.

Figure 5 shows the total volume of sediment excavated from debris basins (Figure 5a) and flood channels (Figure 5b) per century under the each of the maintenance models. The volume of sediment removed from debris basins increases with more intensive maintenance practices, and this results in a decrease in the amount

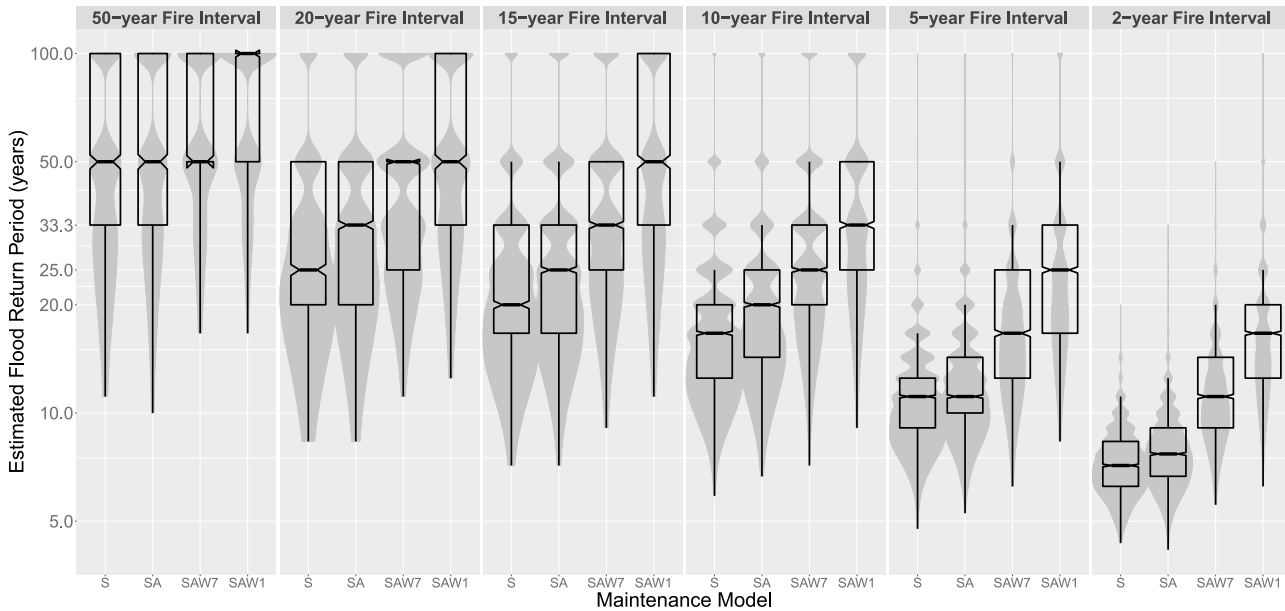

Figure 4. Simulated distributions of flood return period versus infrastructure maintenance approach (S, SA, SAW, and SA1) and fire interval.

of sediment removed from flood channels. The median sediment volume removed from the debris basin across fire frequencies for the SAW1 maintenance scenario was approximately 2.2 times greater than that of the S maintenance scenario. As a result, about 52% less sediment needed to be removed from the channel under the SAW1 scenario than under the S scenario. Figure 5 also shows that the amount of sediment that needs to be excavated from infrastructure per century increases dramatically with decreasing fire interval: under the 2-year fire interval scenario, the amount of sediment removed from the debris basin was 9.7 times greater and the amount removed from the flood channel 12 times greater than that under the 50-year fire interval scenario across all maintenance approaches.

3.3. Flood and Debris Hazards Versus Burn Severity

Attention now turns to the influence of burn severity on flood return periods, which enters the modeling framework through the bulking factor, k. Figure 6 shows T_c distributions across the four *infrastructure design standards* (50C, 100C, 50B, and 100B) and three different levels of *burn severity* (Low, Moderate, and High). Figure 6 shows that with increasing burn severity, flood return periods are reduced. For example, in the case of Moderate Burn Severity, infrastructure designed based on a 100-year design storm and bulked design discharge (100B), the most conservative design standard considered, delivers protection corresponding to a 100-year return period, based on the median value. In transitioning from Moderate to High Burn Severity, the median T_c for design standard 100B is reduced from 100 to 33.3 years, corresponding to a threefold increase in flood frequency.

Figure 7 shows T_c distributions across the four *maintenance approaches* (S, SA, SAW7, and SAW1) and three different levels of *burn severity* (Low, Moderate, and High). These simulations are based on infrastructure designed with a 50-year bulked (50B) design standard, and for cases of Low Burn Severity, that level of protection is exceeded under all maintenance approaches: the median value of T_c is 100 years or greater in all cases. With Moderate Burn Severity, the median value of the simulated T_c distribution is 50 years based on the summer-only cleaning model (S) and increases to 100 years with the three other maintenance models. And finally, the case of High Burn Severity, the median T_c falls to 25 years for the summer cleaning scenarios (S and SA) and to 33.3 years for the SAW7 scenario, but retains the 50-year level of protection using the SAW1 maintenance approach. In the case of the High Burn Severity, the level of bulking is much higher than that assumed for infrastructure design purposes ($k_{des} = 1.2$), which leads to a major reduction in the level of infrastructure performance compared to that of the Low and Moderate Burn Severity scenarios.

10.1029/2022EF002670

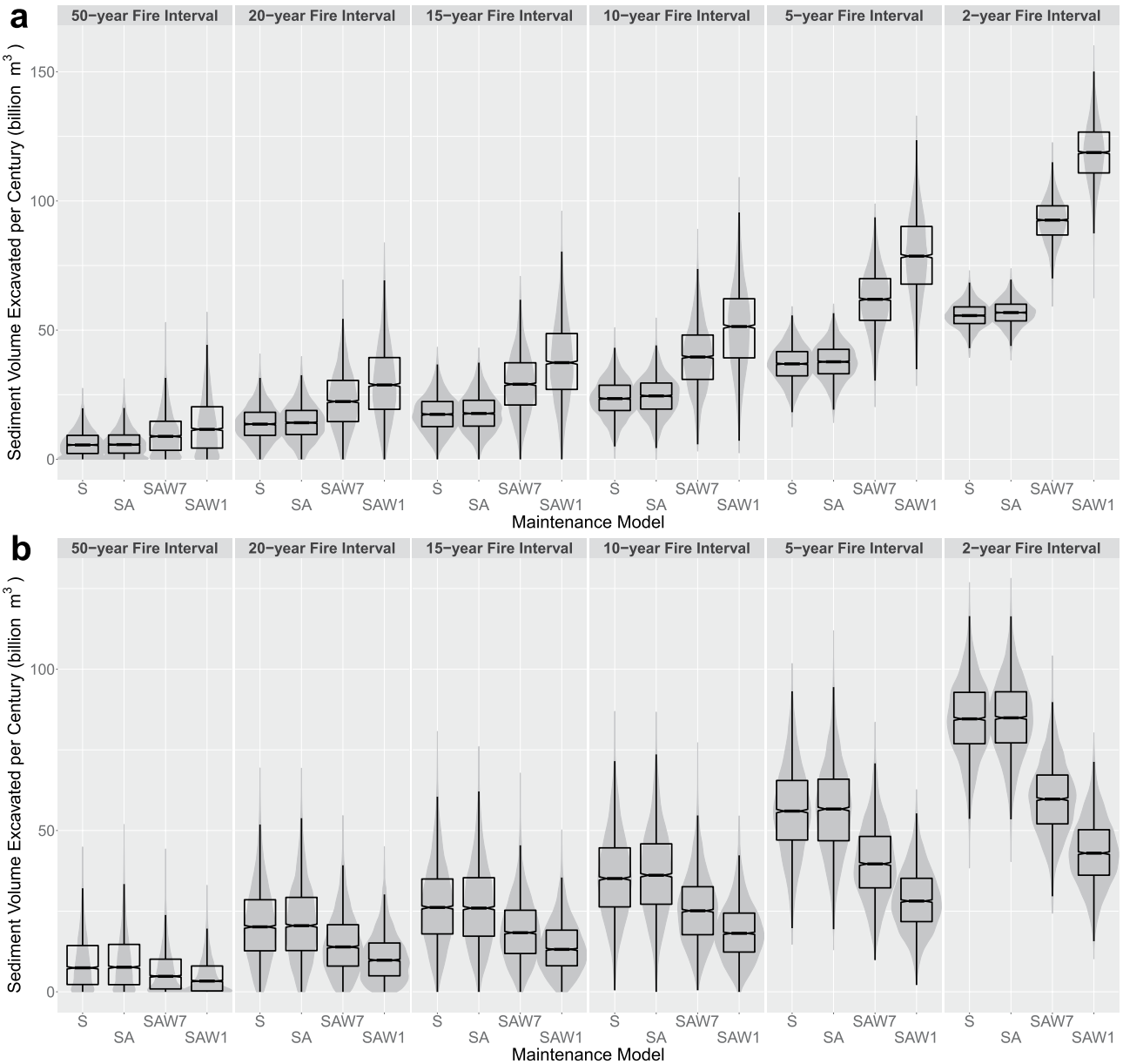

Figure 5. Simulated distributions of sediment volume removed from (a) debris basins and (b) flood channels per century versus maintenance approach (S, SA, SAW7, and SAW1) and fire interval.

4. Discussion

The previous results clearly show that peak bulked flows may exceed the capacities of channels located below burn areas at frequencies far greater than inferred by the exceedance probability of precipitation used for infrastructure design. To this end, we define a hazard amplification factor,

$$A_F = T_p/T_c = p_c/p_p \tag{24}$$

which represents a ratio of the *frequency* of overtopping events for the marginal hazard (precipitation in the absence of wildfire) to that of the compound hazard. Results presented here point to hazard amplification factors ranging from 1.0 to 16.0 across all simulation scenarios.

To get a sense of present post-fire flood risks, consider the range of hazard amplification factors that results from scenarios combining the 50 and 100B design standards with the range of historically observed fire intervals in

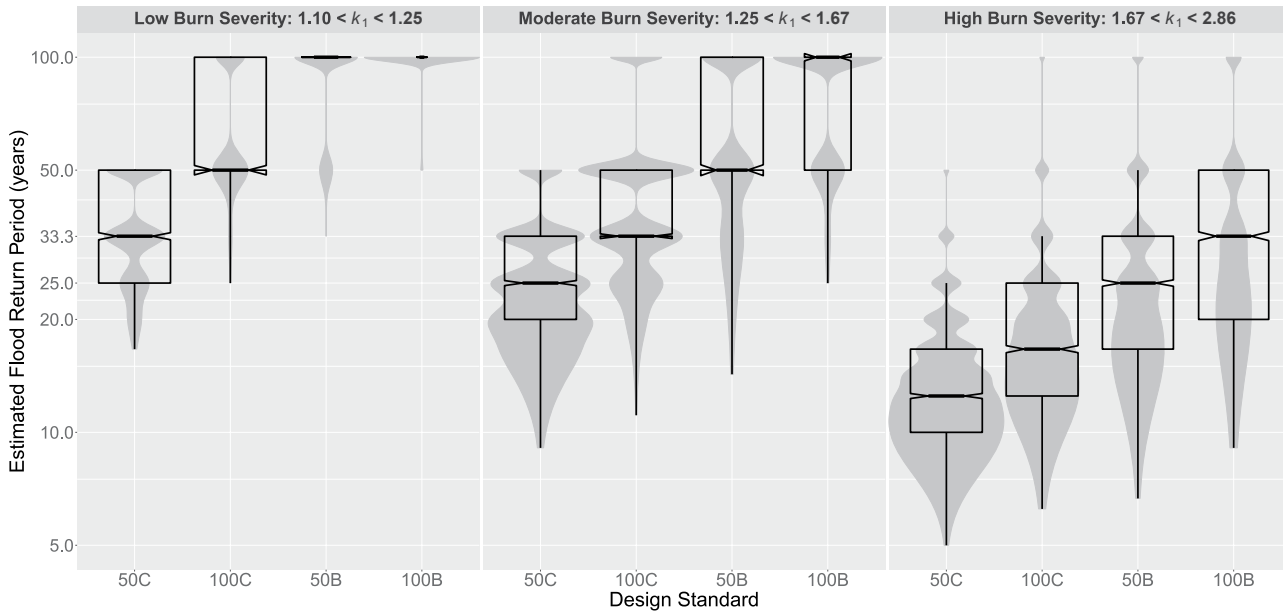

Figure 6. Simulated distributions of flood return period versus infrastructure design standard (50C, 50B, 100C, and 100B) and fire burn severity (Low, Moderate, and High). Missing values are due to a lack of annual channel exceedances during simulation trials.

southern California, 7–52 years (USDA Forest Service, 2012): the median hazard amplification factors are 1.0, 2.0, 4.0, and 6.0 for the 50B/52-year scenario, 100B/52-year scenario, 50B/7-year scenario, and 100 B/7-year scenario, respectively. For context, we note that the 50B design standard is a generalized representation of the design standard used by Los Angeles County (LACDPW, 2006a; LACDPW, 2006b), which operates nearly 200 debris basins across the county.

Now consider future scenarios in which the fire interval decreases to 5 or 2 years, resulting in median amplification factors of 4.5 and 7.0 for the 50B design standard and 7.0 and 11 for the 100B design standard, respectively (Figure 3). These constitute compound hazard estimates up to an order of magnitude greater than the return

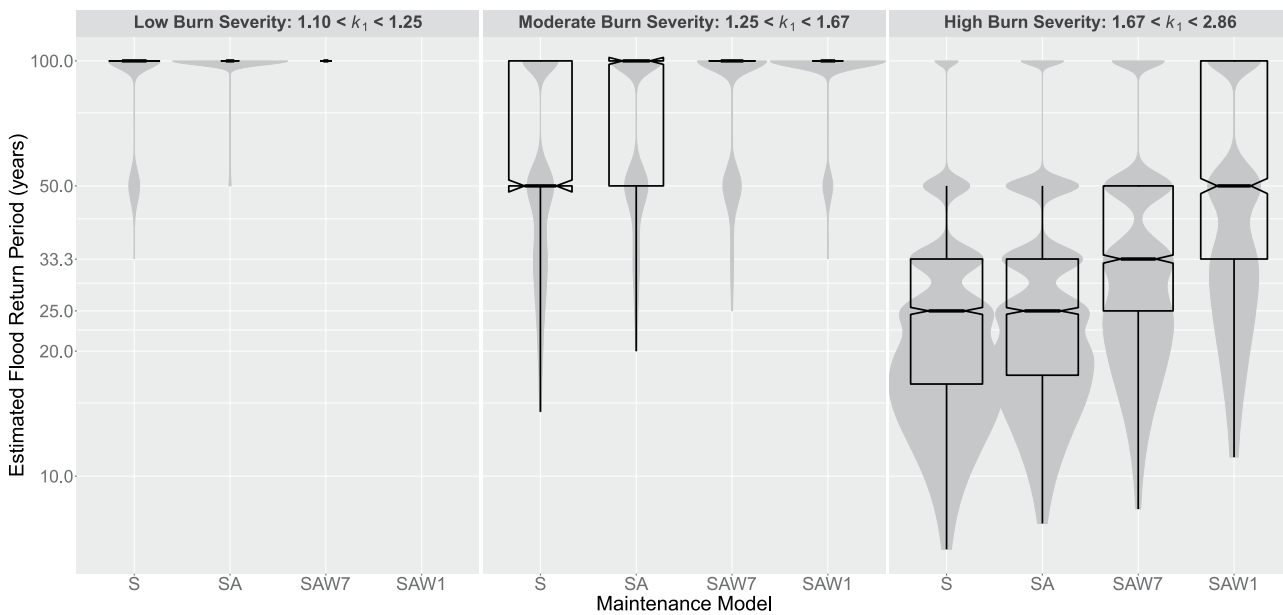

Figure 7. Simulated distributions of flood return period versus infrastructure maintenance approach (S, SA, SAW7, and SAW1) and fire burn severity (Low, Moderate, and High). Missing values are due to a lack of annual channel exceedances during simulation trials.

period for which the flood infrastructure is designed. With respect to our choice of 2 years for the lower bound of the fire interval, we do not expect fire intervals in the region to decrease below this value based on projections of future fire intervals and a review of post-fire watershed recovery in Mediterranean climates that found a minimum recovery period of 2 years (Gao et al., 2021; Wagenbrenner et al., 2021). This simple comparison demonstrates the potential of the modeling framework to predict future hazards based on any distribution of hazard drivers (e.g., fire interval, fire severity, precipitation intensity, and changes in maintenance). Previous studies have documented the value of stochastic modeling for studying infrastructure performance (Byun & Hamlet, 2020), and there is growing interest in understanding non-stationarity in flood hazards. For example, non-stationarity in flood hazards has been linked to land use or land cover change (Luke et al., 2017), sea level rise (Wahl et al., 2017), and more intense precipitation extremes (Brunner et al., 2021; Swain et al., 2018). However, predicting future distributions of hazard drivers is not straightforward. For example, projections of future precipitation have proven challenging, especially for California (Huang et al., 2020). That said, our model can be used to determine the consequences of assuming a particular distribution for a given hazard driver on the post-fire flood hazard, which may prove useful to flood management agencies until the uncertainty in projections is reduced.

The design and construction of flood infrastructure, as well as its maintenance, are affected by many factors including available financial resources and government permit requirements. Maintenance costs for infrastructure cleaning generally scale with the volume of material to be excavated, and the timing of the excavation. Excavation during the wet season may be several times more expensive than dry season excavation due to the physical processing required of wet sediment and mud, the challenge of finding a disposal site, and other factors (RCFCWCD, 2021). Modeling results show the volumes of material requiring excavation increase by about an order of magnitude as fire interval decreases from 50 to 20 years (Figure 5). Furthermore, simulations show that the volumes of material requiring excavation from channels decrease as excavation of debris basins becomes more aggressive. Our model produces quantitative estimates of the magnitude of excavation required to maintain flood infrastructure performance that could help flood management agencies evaluate the cost-effectiveness of different maintenance approaches under multiple climate change scenarios and multidecadal planning timescales.

Increased awareness of hazard amplification among exposed populations could prove especially valuable for public safety. Given the short time period between wildfire containment in Summer or Fall and potential precipitation-induced flooding and debris flows in Winter or Spring, emergency responders and residents of the wildland-urban interface could be fatigued from fire mitigation and evacuation and less able to respond quickly to post-fire flooding and debris flows. Furthermore, residents who trust that debris basins and flood control channels will be sufficient to contain post-fire runoff and who are unaware of potential overtopping could be relatively unconcerned about flooding and debris hazards and be less prepared to respond (Houston et al., 2019; Hutton et al., 2019; Montz & Tobin, 2008). In addition, post-wildfire debris flows can travel with surprising speed several kilometers from the burn area, impacting unexpecting residents of the urbanized lowlands who in many cases may be of a lower socioeconomic status with fewer resources to respond compared to residents on higher ground along the wildland-urban interface (Figure 1). Impacts on lowland residents could be particularly severe if sediment fluxes clog downstream flood control infrastructure resulting in unpredictable flow paths through these communities. For these reasons, advancing a greater understanding about hazard amplification and the potential limitations of flood control protections among emergency agencies and residents of these areas will be very important given the expected intensification of fire and storm events in coming years.

5. Conclusion

In this study, a new modeling framework is developed for estimation of compound post-fire flood hazards below mountain catchments based on multiple interdependent factors including the frequency and severity of wildfires, the effect of wildfire on sediment production and flood peaks, the presence of debris basins and flood channels to mitigate hazards, the loss of channel capacity from sedimentation and clogging, and the restoration of channel capacity with infrastructure maintenance. Compound hazards are estimated by counting overtopping events within century-long Monte Carlo simulations with stochastic inputs. While the model is applied here with parameters representative of southern California, it can be parameterized for other regions, making it highly transferable.

Application of the model shows that the hazard facing human populations may be up to an order of magnitude greater than what would be expected based on the return period of the primary hazard driver (rainfall) used for infrastructure design. Moreover, we find that this hazard amplification is sensitive to design standards. For example, in southern California where fire intervals are roughly 20 years on average, infrastructure designed based on extreme rainfall with a 50-year return period yields a level of protection corresponding to a 15-year or 25-year return period depending on whether a clear-water (50C) or bulked flow (50B) design approach is used, respectively. This corresponds to a hazard amplification of 2.0–3.3. Similarly, designs based on extreme rainfall with a 100-year return period yields a level of protection corresponding to roughly 20-year and 30-year return periods depending on whether a clear-water (100C) or bulked flow (100B) design approach is used. This corresponds to a hazard amplification of 3.3–5.0. Considering that the 50 and 100B design standard scenarios were based on infrastructure design standards currently used by two highly populated counties in southern California, these hazard amplification factors point to concerning limitations to the protection of human development from post-fire flood risk.

Simulations also show that differing maintenance approaches influence hazard amplification. For example, with a 20-year fire interval and a 50-year bulked design standard, the flood return period can range from 25 to 50 years across the four maintenance scenarios based on operational maintenance approaches in Riverside County. This corresponds to a hazard amplification of 2.0 and 1.0, respectively.

Stochastic simulations also reveal the sensitivity of compound post-fire flood hazards to a prominent aspect of the effects of climate change in southern California, increased wildfire frequency. For example, if fire intervals were to shift from 20 to 10 years, the median flood return period for the 50-year bulked flow design approach would be reduced from 25 to 17 years. Hence, the hazard amplification would increase from 2.0 to 3.0. Furthermore, simulations show that shifts in burn severity also increase the hazard amplification. For example, infrastructure that is constructed based on a 50-year bulked flow design standard and experiences only moderate burn severity events (which match the design standard) exhibit a 50-year level of protection, but a shift to high burn severity reduces the flood return period to 25 years, corresponding to a hazard amplification of 2.0.

The ability of this original modeling framework to quantify compound post-fire flood hazards as a function of wildfire severity and frequency, precipitation intensity, and flood infrastructure design and maintenance makes it a useful tool for risk management. In particular, model applications can support flood risk communication efforts to increase awareness of the heightened flood hazards. Furthermore, the model could be applied to back-calculate the sizing of infrastructure and maintenance levels needed to achieve a specific standard of protection, such as a 50-year return period.

Data Availability Statement

After the embargo period, the data and model scripts will be made available in the open repository DRYAD (https://doi.org/10.7280/D16Q59). The precipitation record used to develop the stochastic rainfall model was retrieved from the Climate Data Online database (NOAA, n.d.). MATLAB (MATLAB, 2021) was used to develop the model and to conduct the majority of the statistical analysis of the observed data and the simulation results. R (R Core Team, 2021) was used to generate boxplot visualizations and for minor data analysis.

Acknowledgments
The authors gratefully acknowledge Riverside County Flood Control and Water Conservation District for providing access to data and knowledge about flood management that greatly contributed to this research. This material is based upon work supported by the National Science Foundation under Grant HDBE-2031535. This work was also supported by the NOAA Effects of Sea Level Rise Program under Grant NA16NOS4780206, and by the Ridge to Reef NSF Research Traineeship, award DGE-1735040.

References

Adane, G. B., Hirpa, B. A., Lim, C.-H., & Lee, W.-K. (2020). Spatial and temporal analysis of dry and wet spells in upper awash river basin, Ethiopia. *Water*, *12*(11), 3051. https://doi.org/10.3390/w12113051

Armanini, A., Fraccarollo, L., & Rosatti, G. (2009). Two-dimensional simulation of debris flows in erodible channels. *Computers & Geosciences*, *35*(5), 993–1006. https://doi.org/10.1016/j.cageo.2007.11.008

Brand, M. W., Gudiño-Elizondo, N., Allaire, M., Wright, S., Matson, W., Saksa, P., & Sanders, B. F. (2020). Stochastic hydro-financial watershed modeling for environmental impact bonds. *Water Resources Research*, *56*(8), e2020WR027328. https://doi.org/10.1029/2020wr027328

Brunner, M. I., Swain, D. L., Wood, R. R., Willkofer, F., Done, J. M., Gilleland, E., & Ludwig, R. (2021). An extremeness threshold determines the regional response of floods to changes in rainfall extremes. *Communications Earth & Environment*, *2*(1), 1–11. https://doi.org/10.1038/s43247-021-00248-x

Byun, K., & Hamlet, A. F. (2020). A risk-based analytical framework for quantifying non-stationary flood risks and establishing infrastructure design standards in a changing environment. *Journal of Hydrology*, *584*, 124575. https://doi.org/10.1016/j.jhydrol.2020.124575

Cannon, S. H., & DeGraff, J. (2009). The increasing wildfire and post-fire debris-flow threat in Western USA, and implications for consequences of climate change. In *Landslides–disaster risk reduction* (pp. 177–190). Springer.

Cannon, S. H., Gartner, J. E., Rupert, M. G., Michael, J. A., Rea, A. H., & Parrett, C. (2010). Predicting the probability and volume of postwildfire debris flows in the intermountain Western United States. *GSA Bulletin*, *122*(1–2), 127–144. https://doi.org/10.1130/b26459.1

Chen, L., Berli, M., & Chief, K. (2013). Examining modeling approaches for the rainfall-runoff process in wildfire-affected watersheds: Using san dimas experimental forest. *Journal of the American Water Resources Association*, *49*(4), 851–866. https://doi.org/10.1111/jawr.12043

Christen, M., Kowalski, J., & Bartelt, P. (2010). RAMMS: Numerical simulation of dense snow avalanches in three-dimensional terrain. *Cold Regions Science and Technology*, *63*(1–2), 1–14. https://doi.org/10.1016/j.coldregions.2010.04.005

Cutter, S. L., Emrich, C. T., Gall, M., & Reeves, R. (2018). Flash flood risk and the paradox of urban development. *Natural Hazards Review*, *19*(1), 05017005. https://doi.org/10.1061/(asce)nh.1527-6996.0000268

Dennison, P. E., Brewer, S. C., Arnold, J. D., & Moritz, M. A. (2014). Large wildfire trends in the Western United States, 1984–2011. *Geophysical Research Letters*, *41*(8), 2928–2933. https://doi.org/10.1002/2014gl059576

Finney, M. A. (2005). The challenge of quantitative risk analysis for wildland fire. *Forest Ecology and Management*, *211*(1–2), 97–108. https://doi.org/10.1016/j.foreco.2005.02.010

Gao, P., Terando, A. J., Kupfer, J. A., Varner, J. M., Stambaugh, M. C., Lei, T. L., & Hiers, J. K. (2021). Robust projections of future fire probability for the conterminous United States. *Science of the Total Environment*, *789*, 147872. https://doi.org/10.1016/j.scitotenv.2021.147872

Gartner, J. E., Cannon, S. H., Helsel, D. R., & Bandurraga, M. (2009). Multivariate statistical models for predicting sediment yields from southern California watersheds. *Tech. Rep. Citeseer*. https://doi.org/10.3133/ofr20091200

Gartner, J. E., Cannon, S. H., & Santi, P. M. (2014). Empirical models for predicting volumes of sediment deposited by debris flows and sediment-laden floods in the transverse ranges of southern California. *Engineering Geology*, *176*, 45–56. https://doi.org/10.1016/j.enggeo.2014.04.008

Gershunov, A., Shulgina, T., Clemesha, R. E., Guirguis, K., Pierce, D. W., Dettinger, M. D., et al. (2019). Precipitation regime change in Western North America: The role of atmospheric rivers. *Scientific Reports*, *9*(1), 1–11.

Goodrich, D., Burns, I., Unkrich, C., Semmens, D. J., Guertin, D., Hernandez, M., et al. (2012). KINEROS2/AGWA: Model use, calibration, and validation. *Transactions of the ASABE*, *55*(4), 1561–1574.

Gusman, A. J. (2011). *Sediment/debris bulking factors and post-fire hydrology for Ventura county (Tech. Rep.)*. WEST Consultants, Inc. https://s29422.pcdn.co/wp-content/uploads/2019/11/BulkingFactorStudy-DraftCombinedReport5-15-11.pdf

Houston, D., Cheung, W., Basolo, V., Feldman, D., Matthew, R., Sanders, B. F., et al. (2019). The influence of hazard maps and trust of flood controls on coastal flood spatial awareness and risk perception. *Environment and Behavior*, *51*(4), 347–375. https://doi.org/10.1177/0013916517748711

Huang, X., Swain, D. L., & Hall, A. D. (2020). Future precipitation increase from very high resolution ensemble downscaling of extreme atmospheric river storms in California. *Science Advances*, *6*(29), eaba1323. https://doi.org/10.1126/sciadv.aba1323

Hutton, N. S., Tobin, G. A., & Montz, B. E. (2019). The levee effect revisited: Processes and policies enabling development in Yuba county, California. *Journal of Flood Risk Management*, *12*(3), e12469. https://doi.org/10.1111/jfr3.12469

Hyde, K. D., Riley, K., & Stoof, C. (2017). Uncertainties in predicting debris flow hazards following wildfire. Natural hazard uncertainty assessment: Modeling and decision support. *Geophysical Monograph*, *223*, 287–299.

Jakob, M., Hungr, O., & Jakob, D. M. (2005). *Debris-flow hazards and related phenomena* (Vol. 739). Springer.

Jennings, P. C., & Brooks, N. H. (1982). Storms, Floods, and Debris Flows in Southern California and Arizona, 1978 and 1980: Proceedings of a Symposium, September 17-18, 1980. National Academy Press.

Johnson, P. A., & McCuen, R. H. (1992). Effect of debris flows on debris basin design. *Critical Reviews in Environmental Science and Technology*, *22*(1–2), 137–149. https://doi.org/10.1080/10643389209388431

Johnson, P. A., McCuen, R. H., & Hromadka, T. V. (1991). Debris basin policy and design. *Journal of Hydrology*, *123*(1–2), 83–95. https://doi.org/10.1016/0022-1694(91)90070-x

Kampf, S. K., Brogan, D. J., Schmeer, S., MacDonald, L. H., & Nelson, P. A. (2016). How do geomorphic effects of rainfall vary with storm type and spatial scale in a post-fire landscape? *Geomorphology*, *273*, 39–51. https://doi.org/10.1016/j.geomorph.2016.08.001

Kean, J. W., & Staley, D. M. (2021). Forecasting the frequency and magnitude of postfire debris flows across southern California. *Earth's Future*, *9*(3), e2020EF001735. https://doi.org/10.1029/2020ef001735

Kean, J. W., Staley, D. M., Lancaster, J. T., Rengers, F. K., Swanson, B. J., Coe, J. A., et al. (2019). Inundation, flow dynamics, and damage in the 9 January 2018 Montecito debris-flow event, California, USA: Opportunities and challenges for post-wildfire risk assessment. *Geosphere*, *15*(4), 1140–1163. https://doi.org/10.1130/ges02048.1

Kinoshita, A. M., Hogue, T. S., & Napper, C. (2014). Evaluating pre-and post-fire peak discharge predictions across Western us watersheds. *Journal of the American Water Resources Association*, *50*(6), 1540–1557. https://doi.org/10.1111/jawr.12226

Kroese, D. P., Brereton, T., Taimre, T., & Botev, Z. I. (2014). Why the Monte Carlo method is so important today. *Wiley Interdisciplinary Reviews: Computational Statistics*, *6*(6), 386–392. https://doi.org/10.1002/wics.1314

LACDPW. (2006a). *Hydrology manual (Tech. Rep.)*. Los Angeles County Department of Public Works. Retrieved from https://dpw.lacounty.gov/wrd/publication/engineering/2006_Hydrology_Manual/2006%20Hydrology%20Manual-Divided.pdf

LACDPW. (2006b). *Sedimentation manual (Tech. Rep.)*. Los Angeles County Department of Public Works. Retrieved from https://dpw.lacounty.gov/wrd/publication/engineering/2006_sedimentation_manual/Sedimentation%20Manual-Second%20Edition.pdf

Lavé, J., & Burbank, D. (2004). Denudation processes and rates in the transverse ranges, southern California: Erosional response of a transitional landscape to external and anthropogenic forcing. *Journal of Geophysical Research*, *109*(F1). https://doi.org/10.1029/2003jf000023

Li, J., Cao, Z., Hu, K., Pender, G., & Liu, Q. (2018). A depth-averaged two-phase model for debris flows over erodible beds. *Earth Surface Processes and Landforms*, *43*(4), 817–839. https://doi.org/10.1002/esp.4283

Li, S., & Banerjee, T. (2021). Spatial and temporal pattern of wildfires in California from 2000 to 2019. *Scientific Reports*, *11*(1), 1–17. https://doi.org/10.1038/s41598-021-88131-9

Littell, J. S., Peterson, D. L., Riley, K. L., Liu, Y., & Luce, C. H. (2016). A review of the relationships between drought and forest fire in the United States. *Global Change Biology*, *22*(7), 2353–2369. https://doi.org/10.1111/gcb.13275

Liu, K.-F., & Huang, M. C. (2006). Numerical simulation of debris flow with application on hazard area mapping. *Computational Geosciences*, *10*(2), 221–240. https://doi.org/10.1007/s10596-005-9020-4

Luke, A., Sanders, B. F., Goodrich, K. A., Feldman, D. L., Boudreau, D., Eguiarte, A., et al. (2018). Going beyond the flood insurance rate map: Insights from flood hazard map co-production. *Natural Hazards and Earth System Sciences*, *18*(4), 1097–1120. https://doi.org/10.5194/nhess-18-1097-2018

Luke, A., Vrugt, J. A., AghaKouchak, A., Matthew, R., & Sanders, B. F. (2017). Predicting nonstationary flood frequencies: Evidence supports an updated stationarity thesis in the United States. *Water Resources Research*, *53*(7), 5469–5494. https://doi.org/10.1002/2016wr019676

Majd, M. S., & Sanders, B. F. (2014). The LHLLC scheme for two-layer and two-phase transcritical flows over a mobile bed with avalanching, wetting and drying. *Advances in Water Resources*, *67*, 16–31. https://doi.org/10.1016/j.advwatres.2014.02.002

Martínez-Aranda, S., Murillo, J., & García-Navarro, P. (2022). A GPU-accelerated efficient simulation tool (EST) for 2d variable-density mud/debris flows over non-uniform erodible beds. *Engineering Geology*, *296*, 106462. https://doi.org/10.1016/j.enggeo.2021.106462

MATLAB. (2021). *Version 9.10.0.1602886 (r2021a)*. The MathWorks Inc.

Mayor, Á. G., Bautista, S., & Bellot, J. (2011). Scale-dependent variation in runoff and sediment yield in a semiarid mediterranean catchment. *Journal of Hydrology*, *397*(1–2), 128–135. https://doi.org/10.1016/j.jhydrol.2010.11.039

Meyer, G. A., & Wells, S. G. (1997). Fire-related sedimentation events on alluvial fans, Yellowstone National Park, USA. *Journal of Sedimentary Research*, *67*(5), 776–791.

Meyer, G. A., Wells, S. G., & Timothy Jull, A. (1995). Fire and alluvial chronology in Yellowstone National Park: Climatic and intrinsic controls on holocene geomorphic processes. *The Geological Society of America Bulletin*, *107*(10), 1211–1230. https://doi.org/10.1130/0016-7606(1995)107<1211:faaciy>2.3.co;2

Montz, B. E., & Tobin, G. A. (2008). Livin' large with levees: Lessons learned and lost. *Natural Hazards Review*, *9*(3), 150–157. https://doi.org/10.1061/(asce)1527-6988(2008)9:3(150)

Moody, J. A., Shakesby, R. A., Robichaud, P. R., Cannon, S. H., & Martin, D. A. (2013). Current research issues related to post-wildfire runoff and erosion processes. *Earth-Science Reviews*, *122*, 10–37. https://doi.org/10.1016/j.earscirev.2013.03.004

Nadal-Romero, E., Martínez-Murillo, J. F., Vanmaercke, M., & Poesen, J. (2011). Scale-dependency of sediment yield from badland areas in mediterranean environments. *Progress in Physical Geography*, *35*(3), 297–332. https://doi.org/10.1177/0309133311400330

National Research Council. (1996). *Alluvial fan flooding*. National Academies Press.

NOAA. (n.d.). Climate data online search [Dataset]. NOAA. Retrieved from https://www.ncdc.noaa.gov/cdo-web/datasets/GHCND/stations/GHCND:USC00040798/detail

O'Brien, J. S., Julien, P. Y., & Fullerton, W. (1993). Two-dimensional water flood and mudflow simulation. *Journal of Hydraulic Engineering*, *119*(2), 244–261.

Osanai, N., Mizuno, H., & Mizuyama, T. (2010). Design standard of control structures against debris flow in Japan. *Journal of Disaster Research*, *5*(3), 307–314. https://doi.org/10.20965/jdr.2010.p0307

Pelletier, J. D., & Orem, C. A. (2014). How do sediment yields from post-wildfire debris-laden flows depend on terrain slope, soil burn severity class, and drainage basin area? Insights from airborne-lidar change detection. *Earth Surface Processes and Landforms*, *39*(13), 1822–1832. https://doi.org/10.1002/esp.3570

Pierson, T. C. (2005). Hyperconcentrated flow—Transitional process between water flow and debris flow. In *Debris-flow hazards and related phenomena* (pp. 159–202). Springer.

Piton, G., & Recking, A. (2016). Design of sediment traps with open check dams. II: Woody debris. *Journal of Hydraulic Engineering*, *142*(2), 04015046. https://doi.org/10.1061/(asce)hy.1943-7900.0001049

Prochaska, A. B., Santi, P. M., & Higgins, J. D. (2008). Debris basin and deflection berm design for fire-related debris-flow mitigation. *Environmental and Engineering Geoscience*, *14*(4), 297–313. https://doi.org/10.2113/gseegeosci.14.4.297

Radeloff, V. C., Helmers, D. P., Kramer, H. A., Mockrin, M. H., Alexandre, P. M., Bar-Massada, A., et al. (2018). Rapid growth of the us wildland-urban interface raises wildfire risk. *Proceedings of the National Academy of Sciences of the United States of America*, *115*(13), 3314–3319. https://doi.org/10.1073/pnas.1718850115

RCFCWCD. (2021). Personal communication. (Riverside County Flood Control and Water Conservation District).

R Core Team. (2021). R: A language and environment for statistical computing. [Computer software manual]. R Core Team. Retrieved from https://www.R-project.org/dataset

Richardson, C. W. (1981). Stochastic simulation of daily precipitation, temperature, and solar radiation. *Water Resources Research*, *17*(1), 182–190. https://doi.org/10.1029/wr017i001p00182

Rickenmann, D., Laigle, D., McArdell, B., & Hübl, J. (2006). Comparison of 2D debris-flow simulation models with field events. *Computational Geosciences*, *10*(2), 241–264. https://doi.org/10.1007/s10596-005-9021-3

Robichaud, P., Elliot, W., Pierson, F., Hall, D., & Moffet, C. (2007). Predicting postfire erosion and mitigation effectiveness with a web-based probabilistic erosion model. *Catena*, *71*(2), 229–241. https://doi.org/10.1016/j.catena.2007.03.003

Rosatti, G., & Begnudelli, L. (2013). Two-dimensional simulation of debris flows over mobile bed: Enhancing the TRENT2D model by using a well-balanced generalized roe-type solver. *Computers & Fluids*, *71*, 179–195. https://doi.org/10.1016/j.compfluid.2012.10.006

Sadegh, M., Moftakhari, H., Gupta, H. V., Ragno, E., Mazdiyasni, O., Sanders, B., et al. (2018). Multihazard scenarios for analysis of compound extreme events. *Geophysical Research Letters*, *45*(11), 5470–5480. https://doi.org/10.1029/2018gl077317

Sanders, B. F., & Grant, S. B. (2020). Re-envisioning stormwater infrastructure for ultrahazardous flooding. *Wiley Interdisciplinary Reviews: Water*, *7*(2), e1414. https://doi.org/10.1002/wat2.1414

Sanders, B. F., Schubert, J. E., Goodrich, K. A., Houston, D., Feldman, D. L., Basolo, V., et al. (2020). Collaborative modeling with fine-resolution data enhances flood awareness, minimizes differences in flood perception, and produces actionable flood maps. *Earth's Future*, *8*(1), e2019EF001391. https://doi.org/10.1029/2019ef001391

Scott, K. M., & Williams, R. P. (1978). *Erosion and sediment yields in the transverse ranges, southern California* (Vol. 1030). US Government Printing Office.

Shahraki, N., Bakhtiari, B., & Ahmadi, M. (2013). Markov chain model for probability of dry, wet days and statistical analysis of daily rainfall in some climatic zone of Iran. *Aerul si Apa: Compon. ale Mediului*, *4*, 399–416.

Shakesby, R. (2011). Post-wildfire soil erosion in the mediterranean: Review and future research directions. *Earth-Science Reviews*, *105*(3–4), 71–100. https://doi.org/10.1016/j.earscirev.2011.01.001

Sharma, M. A., & Singh, J. B. (2010). Use of probability distribution in rainfall analysis. *New York Science Journal*, *3*(9), 40–49.

Staley, D. M., Kean, J. W., Cannon, S. H., Schmidt, K. M., & Laber, J. L. (2013). Objective definition of rainfall intensity–duration thresholds for the initiation of post-fire debris flows in southern California. *Landslides*, *10*(5), 547–562. https://doi.org/10.1007/s10346-012-0341-9

Staley, D. M., Negri, J. A., Kean, J. W., Laber, J. L., Tillery, A. C., & Youberg, A. M. (2016). *Updated logistic regression equations for the calculation of post-fire debris-flow likelihood in the western United States*. US Department of the Interior, US Geological Survey.

Staley, D. M., Negri, J. A., Kean, J. W., Laber, J. L., Tillery, A. C., & Youberg, A. M. (2017). Prediction of spatially explicit rainfall intensity–duration thresholds for post-fire debris-flow generation in the Western United States. *Geomorphology*, *278*, 149–162. https://doi.org/10.1016/j.geomorph.2016.10.019

Stern, R., & Coe, R. (1984). A model fitting analysis of daily rainfall data. *Journal of the Royal Statistical Society: Series A*, *147*(1), 1–18. https://doi.org/10.2307/2981736

Sumeet, M., Yatnesh, B., Shri, K., Gaurav, S., & Nema, A. (2013). Markov chain model probability of dry wet weeks and statistical analysis of weekly rainfall for agricultural planning at Jabalpur. *Environment and Ecology*, *31*(3), 1250–1254.

Swain, D. L., Langenbrunner, B., Neelin, J. D., & Hall, A. (2018). Increasing precipitation volatility in twenty-first-century California. *Nature Climate Change*, *8*(5), 427–433. https://doi.org/10.1038/s41558-018-0140-y

USDA Forest Service. (2012). Fire return interval in CA, 1908-2012. [Dataset]. USDA. Retrieved from https://www.sciencebase.gov/catalog/item/563be0fbe4b0d6133fe76016

Vahedifard, F., AghaKouchak, A., Ragno, E., Shahrokhabadi, S., & Mallakpour, I. (2017). Lessons from the Oroville dam. *Science*, *355*(6330), 1139–1140. https://doi.org/10.1126/science.aan0171

VCWPD. (2005). *Debris and detention basins (Tech. Rep.).* Ventura County Watershed Protection District. Retrieved from https://s29422.pcdn.co/wp-content/uploads/2019/04/Debris_Basin_Report_VCWPD_2005.pdf

VCWPD. (2017). *Design hydrology manual (Tech. Rep.).* Ventura County Watershed Protection District. Retrieved from https://s29422.pcdn.co/wp-content/uploads/2019/03/Hydrology_Manual_2017Final.pdf

Vieira, D., Fernández, C., Vega, J., & Keizer, J. (2015). Does soil burn severity affect the post-fire runoff and interrill erosion response? A review based on meta-analysis of field rainfall simulation data. *Journal of Hydrology*, *523*, 452–464. https://doi.org/10.1016/j.jhydrol.2015.01.071

Vieira, F. M. C., Machado, J. M. C., de Souza Vismara, E., & Possenti, J. C. (2018). Probability distributions of frequency analysis of rainfall at the southwest region of paraná state, Brazil. *Revista de Ciências Agroveterinárias*, *17*(2), 260–266. https://doi.org/10.5965/223811711722018260

Vogel, R. M. (2017). Stochastic watershed models for hydrologic risk management. *Water Security*, *1*, 28–35. https://doi.org/10.1016/j.wasec.2017.06.001

Wagenbrenner, J. W., Ebel, B. A., Bladon, K. D., & Kinoshita, A. M. (2021). Post-wildfire hydrologic recovery in mediterranean climates: A systematic review and case study to identify current knowledge and opportunities. *Journal of Hydrology*, *602*, 126772. https://doi.org/10.1016/j.jhydrol.2021.126772

Wagenbrenner, J. W., & Robichaud, P. R. (2014). Post-fire bedload sediment delivery across spatial scales in the interior Western United States. *Earth Surface Processes and Landforms*, *39*(7), 865–876. https://doi.org/10.1002/esp.3488

Wahl, T., Haigh, I. D., Nicholls, R. J., Arns, A., Dangendorf, S., Hinkel, J., & Slangen, A. B. (2017). Understanding extreme sea levels for broad-scale coastal impact and adaptation analysis. *Nature Communications*, *8*(1), 1–12. https://doi.org/10.1038/ncomms16075

Wallerstein, N., Thorne, C. R., & Abt, S. R. (1997). Debris control at hydraulic structures in selected areas of the United States and Europe.

Westerling, A. L., Hidalgo, H. G., Cayan, D. R., & Swetnam, T. W. (2006). Warming and earlier spring increase Western us forest wildfire activity. *Science*, *313*(5789), 940–943. https://doi.org/10.1126/science.1128834

Wilks, D. (1998). Multisite generalization of a daily stochastic precipitation generation model. *Journal of Hydrology*, *210*(1–4), 178–191. https://doi.org/10.1016/s0022-1694(98)00186-3

Willardson, B. (2020). Sustainable debris basins for post-fire protection. In *2020 Intermountain Engineering, Technology and Computing (IETC)* (pp. 1–6). https://doi.org/10.1109/ietc47856.2020.9249179

Williams, C. J., Pierson, F. B., Robichaud, P. R., & Boll, J. (2014). Hydrologic and erosion responses to wildfire along the rangeland–xeric forest continuum in the Western US: A review and model of hydrologic vulnerability. *International Journal of Wildland Fire*, *23*(2), 155–172. https://doi.org/10.1071/wf12161

Ye, L., Hanson, L. S., Ding, P., Wang, D., & Vogel, R. M. (2018). The probability distribution of daily precipitation at the point and catchment scales in the United States. *Hydrology and Earth System Sciences*, *22*(12), 6519–6531. https://doi.org/10.5194/hess-22-6519-2018